RESEARCH ARTICLE

Tumefactive Demyelination in MOG Ab–Associated Disease, Multiple Sclerosis, and AQP-4-IgG–Positive Neuromyelitis Optica Spectrum Disorder

Laura Cacciaguerra, MD, Pearse Morris, MBBCh, W. Oliver Tobin, MBBCh, PhD, John J. Chen, MD, PhD, Samantha A. Banks, MD, Paul Elsbernd, MD, Vyanka Redenbaugh, MD, Jan-Mendelt Tillema, MD, Federico Montini, MD, Elia Sechi, MD, A. Sebastian Lopez-Chiriboga, MD, Nicholas Zalewski, MD, Yong Guo, MD, PhD, Maria A. Rocca, MD, Massimo Filippi, MD, Sean J. Pittock, MD, Claudia F. Lucchinetti, MD, and Eoin P. Flanagan, MBBCh

Correspondence
Dr. Flanagan
flanagan.eoin@mayo.edu

Neurology® 2023;100:e1418-e1432. doi:10.1212/WNL.0000000000206820

Abstract

Background and Objectives

Studies on tumefactive brain lesions in myelin oligodendrocyte glycoprotein-immunoglobulin G (IgG)–associated disease (MOGAD) are lacking. We sought to characterize the frequency clinical, laboratory, and MRI features of these lesions in MOGAD and compare them with those in multiple sclerosis (MS) and aquaporin-4-IgG–positive neuromyelitis optica spectrum disorder (AQP4+NMOSD).

Methods

We retrospectively searched 194 patients with MOGAD and 359 patients with AQP4+NMOSD with clinical/MRI details available from the Mayo Clinic databases and included those with ≥1 tumefactive brain lesion (maximum transverse diameter ≥2 cm) on MRI. Patients with tumefactive MS were identified using the Mayo Clinic medical record linkage system. Binary multivariable stepwise logistic regression identified independent predictors of MOGAD diagnosis; Cox proportional regression models were used to assess the risk of relapsing disease and gait aid in patients with tumefactive MOGAD vs those with non-tumefactive MOGAD.

Results

We included 108 patients with tumefactive demyelination (MOGAD = 43; AQP4+NMOSD = 16; and MS = 49). Tumefactive lesions were more frequent among those with MOGAD (43/194 [22%]) than among those with AQP4+NMOSD (16/359 [5%], $p < 0.001$). Risk of relapse and need for gait aid were similar in tumefactive and nontumefactive MOGAD. Clinical features more frequent in MOGAD than in MS included headache (18/43 [42%] vs 10/49 [20%]; $p = 0.03$) and somnolence (12/43 [28%] vs 2/49 [4%]; $p = 0.003$), the latter also more frequent than in AQP4+NMOSD (0/16 [0%]; $p = 0.02$). The presence of peripheral T2-hypointense rim, T1-hypointensity, diffusion restriction (particularly an arc pattern), ring enhancement, and Baló-like or cystic appearance favored MS over MOGAD ($p \leq 0.001$). MRI features were broadly similar in MOGAD and AQP4+NMOSD, except for more frequent diffusion restriction in AQP4+NMOSD (10/15 [67%]) than in MOGAD (11/42 [26%], $p = 0.005$). CSF analysis revealed less frequent positive oligoclonal bands in MOGAD (2/37 [5%]) than in MS (30/43 [70%], $p < 0.001$) and higher median white cell count in MOGAD than in MS (33 vs 6 cells/μL, $p < 0.001$). At baseline, independent predictors of MOGAD diagnosis were the presence of somnolence/headache, absence of T2-hypointense rim, lack of

From the Department of Neurology and Mayo Clinic Center for Multiple Sclerosis and Autoimmune Neurology (L.C., W.O.T., J.J.C., S.A.B., V.R., J.-M.T., Y.G., S.J.P., C.F.L., E.P.F.), Mayo Clinic, Rochester, MN; Vita-Salute San Raffaele University (L.C., F.M., M.A.R., M.F.); Neuroimaging Research Unit (L.C., M.A.R., M.F.), Division of Neuroscience, IRCCS San Raffaele Scientific Institute, Milan, Italy; Department of Radiology (P.M.), Department of Ophthalmology (J.J.C.), Mayo Clinic, Rochester, MN; Department of Neurology (P.E.), San Antonio Military Medical Center, Fort Sam Houston, TX; Neurology Unit (F.M., M.A.R., M.F.), IRCCS San Raffaele Scientific Institute, Milan; Department of Medical, Surgical and Experimental Sciences (E.S.), University of Sassari, Italy; Department of Neurology (A.S.L.-C.), Mayo Clinic, Jacksonville, FL; Department of Neurology (N.Z.), Mayo Clinic, Scottsdale, AZ; Neurorehabilitation Unit (M.F.), IRCCS San Raffaele Scientific Institute; Neurophysiology Service (M.F.), IRCCS San Raffaele Scientific Institute, Milan, Italy; and Laboratory Medicine and Pathology (S.J.P., E.P.F.), Mayo Clinic, Rochester, MN.

Go to Neurology.org/N for full disclosures. Funding information and disclosures deemed relevant by the authors, if any, are provided at the end of the article.

Glossary

aHR = adjusted hazard ratio; **AQP4+NMOSD** = aquaporin-4-IgG–positive neuromyelitis optica spectrum disorders; **DWI** = diffusion-weighted imaging; **EDSS** = Expanded Disability Status Scale; **FLAIR** = fluid-attenuated inversion recovery; **IgG** = immunoglobulin G; **MOG** = myelin oligodendrocyte glycoprotein; **MOGAD** = MOG-IgG–associated disease; **MS** = multiple sclerosis.

T1-hypointensity, and no diffusion restriction (Nagelkerke R^2 = 0.67). Tumefactive lesion resolution was more common in MOGAD than in MS or AQP4+NMOSD and improved model performance.

Discussion

Tumefactive lesions are frequent in MOGAD but not associated with a worse prognosis. The clinical, MRI, and CSF attributes of tumefactive MOGAD differ from those of tumefactive MS and are more similar to those of tumefactive AQP4+NMOSD with the exception of lesion resolution, which favors MOGAD.

Myelin oligodendrocyte glycoprotein (MOG) antibody–associated disease (MOGAD) is a recently defined inflammatory demyelinating disease of the CNS, distinct from multiple sclerosis (MS) and aquaporin-4-immunoglobulin G (IgG)–positive neuromyelitis optica spectrum disorders (AQP4+NMOSD).[1,2] Given the partial clinical overlap of these diseases, with acute attacks involving the brain, optic nerve, and spinal cord, efforts have focused on their radiologic characterization using MRI.

Tumefactive brain lesions (≥2 cm maximum transverse diameter)[3] are a rare but well-recognized manifestation of inflammatory CNS disorders.[4-6] They can be accompanied by severe clinical manifestations (with potential for intensive care unit admission) and often represent a diagnostic challenge for neurologists, especially when encountered in isolation as the initial manifestation of the disease.[7,8]

These lesions have been described in up to 2% of patients with MS,[9] 3% of patients with AQP4+NMOSD,[10] and during MOGAD attacks.[5,11] However, the frequency of this manifestation in MOGAD is still unknown because no studies have systematically evaluated tumefactive demyelination in this disease.

Previous studies identified MRI patterns accompanying tumefactive demyelination and tumefactive MS to distinguish them from alternative nondemyelinating etiologies (e.g., tumors).[4,12] These patterns include a Baló-like appearance, a cystic core, a rim of T2-hypointensity, an arc of restricted diffusion, and a ring or open ring of enhancement.[4,12]

Data on tumefactive demyelination in MOGAD are scarce, but lesions might have different characteristics compared with what is observed in MS and AQP4+NMOSD,[13] assisting in the diagnosis and providing new insights into pathophysiology. Therefore, in this study, we sought to characterize the frequency of tumefactive lesions in patients with MOGAD and the associated clinical, laboratory, and MRI features and outcome, and compare them with those in patients with MS and AQP4+NMOSD.

Methods

Standard Protocol Approvals, Registrations, and Patient Consents

The study was approved by the Mayo Clinic institutional review board (IRB 08-006647). All patients aged 18 years or older and the guardians of pediatric patients gave written consent to the passive use of their medical records for research purposes.

Identification of Patients With MOGAD

We searched our MOGAD databases from January 1, 1996, to September 1, 2020 (including both adults and pediatric patients) and identified 194 patients with clinical and MRI details available. Then, we included those who: (1) had at least 1 tumefactive T2-hyperintense lesion (maximum transverse diameter ≥2 cm)[3]; (2) fulfilled current MOGAD criteria[14] and showed negative results for AQP4-IgG. The remaining patients with nontumefactive MOGAD were used as a control group to assess the cumulative risk of relapsing disease and disability in patients with MOGAD with tumefactive lesions.

Identification of the Comparison Groups

Patients with AQP4+NMOSD and MS were identified with 2 different methodologies. We searched our AQP4+NMOSD database (including both adults and pediatric patients) from January 1, 2000, to August 31, 2020, and found 359 patients with clinical and MRI data available. We included those who had at least 1 tumefactive T2-hyperintense lesion (maximum transverse diameter ≥2 cm), fulfilled 2015 diagnostic criteria for NMOSD with AQP4-IgG,[15] and showed negative results for MOG-IgG.

For patients with MS, we searched the Mayo Clinic electronic medical record for consecutive patients seen from January 1,

2018, to December 31, 2020, with an *International Classification of Diseases, Tenth Revision* (*ICD10*) diagnosis of MS (G35) and "tumefactive" term present in the chart through natural language search, and this identified 42 patients. A further 7 patients were identified from a pediatric MS database. Patients had at least 1 T2-lesion of maximum transverse diameter ≥2 cm, fulfilled 2017 revised diagnostic criteria,[16] and showed negative results for both MOG-IgG and AQP4-IgG.

Antibody Testing

The analyzed serum and CSF samples were fresh or stored. All patients with MOGAD were seropositive for MOG-IgG$_1$ tested in the Mayo Clinic Neuroimmunology Laboratory using a live cell-based assay expressing full-length native conformation human MOG with a cutoff IgG binding index of ≥2.5 and end titration of ≥1:20, as previously described.[17] When available, we also reported the end antibody titer, obtained with progressive dilutions of 1:20, 1:40, 1:100, 1:1,000, and 1:10,000.[17] End titers were stratified as low (1:20 or 1:40) or high (≥1:100). When available, MOG-IgG was tested in the CSF by fluorescence-activated cell sorting assay. AQP4-IgG was tested with live or fixed cell-based assays as previously described.[18,19]

Collection of Demographic, Clinical, and CSF Data

Two neurologists (L.C. and E.P.F.) abstracted from medical records the following demographic and clinical data of patients: age, sex, disease duration, Expanded Disability Status Scale (EDSS)[20] at nadir, neurologic manifestations, the presence of somnolence, vomiting or nausea, headache, and seizures.

CSF data included the detection of oligoclonal bands at any time (including the tumefactive attack), while white blood cell count, protein, and glucose levels were only collected when within 30 days of the attack with the tumefactive lesion(s). We also collected information on whether patients underwent brain biopsy and treatment at follow-up.

Long-term Prognosis of Patients With MOGAD With Tumefactive Lesions

To assess the long-term prognosis of patients with tumefactive MOGAD, the occurrence and timing of relapsing disease course, need of a gait aid (i.e., EDSS milestone of 6), and death among our MOGAD cohort with and without tumefactive lesions were also collected.

MRI Analysis

In each brain MRI scan, we identified the largest tumefactive lesion as the "index lesion" on the fluid-attenuated inversion recovery (FLAIR) sequence or T2-weighted sequence. For each MRI scan, we evaluated FLAIR and/or T2-weighted sequences, diffusion-weighted images, and precontrast and postcontrast T1-weighted sequences at Mayo Clinic or outside facilities. In patients with more than 1 attack associated with a tumefactive lesion, the first one was included in the cross-sectional analysis (i.e., differential diagnosis of tumefactive lesions).

Lesion Location

Lesions were classified according to their location into periventricular lesions (ovoid lesions with the maximum diameter perpendicular to the lateral ventricles and in direct contact with them[21] or any-shaped periventricular lesions), involving other hemispheric white matter, deep gray matter, corticospinal tract, corpus callosum, or infratentorial region.

Index Lesion Characteristics

Index lesions were independently assessed by a neurologist (L.C.) and a neuroradiologist (P.P.M.), blinded to patients' diagnosis. When there was disagreement, a third blinded reviewer (E.P.F.) evaluated images in an anonymous fashion for consensus. The definition and pictorial explanation of features evaluated are reported in Figure 1 and included the presence of the following: (1) T2-hypointense rim on T2-weighted image,[22] (2) T1-hypointensity on T1-weighted image,[4] (3) Baló-like appearance,[23] (4) cystic component,[24] (5) poorly demarcated borders (i.e., fluffy appearance),[25] (6) restricted diffusion within the lesion,[26] (7) arc/ring of peripheral restricted diffusion,[12] (8) enhancement on postcontrast T1-weighted images, (9) pattern of enhancement on postcontrast T1-weighted images including ring (closed if complete; otherwise, open)[22] and cloud-like,[27] and (10) mass effect (i.e., if the lesion exerted a secondary effect on adjacent structures such as sulci, ventricles, or midline).

Index Lesion Size and Number of T2-Hyperintense and Enhancing Lesions

Additional MRI parameters were recorded or measured including the maximum diameter (cm) of the index tumefactive lesion, total number of T2-hyperintense lesions, total number of contrast-enhancing lesions, presence of concomitant multiple tumefactive lesions, and total number of tumefactive lesions.

Lesion Evolution and Subsequent Tumefactive Attacks

When available, we analyzed the first follow-up MRI scan, at least 3 months from the tumefactive attack, and the last available follow-up MRI scan to assess for a complete resolution of the index tumefactive lesion on T2-weighted or T1-weighted images. In those with multiple tumefactive lesions, we compared the MRIs of initial and subsequent tumefactive lesions.

Statistical Analysis

We used Kaplan-Meier survival curves with patients with MOGAD censored according to their follow-up to represent the cumulative risk of relapses or EDSS of 6 over 10 years of disease duration. Proportional Cox regression models with time to relapse as outcome, adjusted for age at onset (continuous variable) and sex (binary variable), were

Figure 1 Pictorial Overview of the MRI Features Evaluated in This Study, With Corresponding Definitions

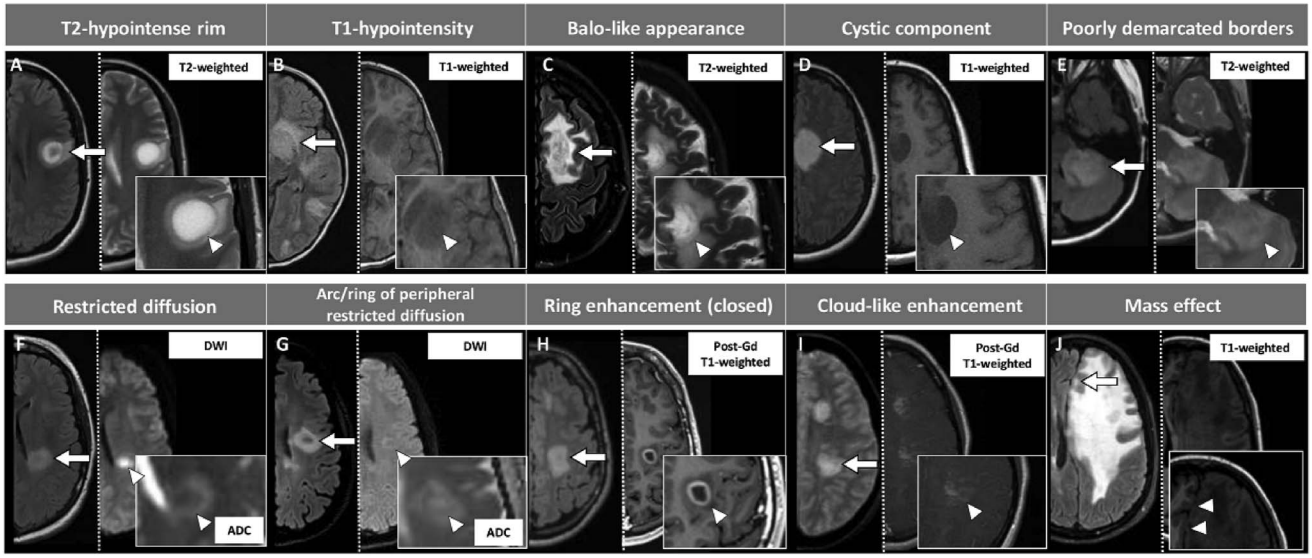

Lesions are shown by arrows and are displayed on axial T2-FLAIR (left half of each image) and on the most appropriate sequence for the evaluation of each specific feature, indicated by an arrowhead (right half of each image). Exceptions are images E and J, where the second sequence (T2-weighted image in E, and T1-weighted image in J) is reported for descriptive purposes only because the T2-FLAIR sequence is suitable for the visualization of those features. For image I, T2-FLAIR image was unavailable and therefore substituted with T2-weighted sequence. Features were defined as follows: (A) T2-hypointense rim: rim-shaped relative T2-hypointensity compared with the T2-hyperintensity of the lesion center and surrounding edema; (B) T1-hypointensity: hypointensity on T1-weighted images compared with the normal-appearing white matter; (C) Baló-like appearance: the presence of ≥2 concentric rings or a pattern of alternating bands of signal intensity on any MRI sequence; (D) cystic component: T2-weighted or T1-weighted signal of similar intensity to CSF; (E) poorly demarcated borders: fluffy appearance on T2-FLAIR or T2-weighted sequences; (F) restricted diffusion: DWI hyperintensity with corresponding hypointensity on the ADC map; (G) arc/ring of peripheral restricted diffusion: dark peripheral ADC arc or ring with a brighter center; (H) ring enhancement (closed ring shown in this figure): circular border of enhancement, closed if complete, otherwise open; (I) cloud-like enhancement: multiple patchy enhancement with ill-defined margins; (J) mass effect: lesion exerting a secondary effect on adjacent structures such as sulci, ventricles, or midline. ADC = apparent diffusion coefficient map; DWI = diffusion-weighted images; FLAIR = fluid-attenuated inversion recovery; Gd = gadolinium.

run to calculate adjusted hazard ratio (aHR) and corresponding 95% CIs.

Between-group comparisons of continuous variables were assessed by using the Kruskal-Wallis test or the independent sample *t* test, according to the normality assumption. For categorical variables, comparisons were performed with the χ^2 tests or the Fisher exact test, as appropriate. An exploratory between-group comparison of clinical and radiologic features of patients with MOGAD according to the age at onset was similarly performed.

A p value of <0.05 was considered significant. To identify clinical and MRI variables associated with MOGAD diagnosis, we first ran univariable binary logistic regression models and then the significant variables (i.e., those significantly associated with MOGAD vs other demyelinating disorders) were included in a binary multivariable stepwise logistic regression (forward selection: likelihood ratio). If separation was encountered, we excluded or merged similar features, as described further.

Data Availability

Anonymized data used for this study are available upon reasonable request from the corresponding author.

Results

Frequency of Tumefactive Lesions in MOGAD

We included 43 patients with MOGAD. The frequency of at least 1 tumefactive brain lesion among the total MOGAD cohort was 22% (43 of 194) and even higher when only patients with inflammatory brain lesions were considered (43 of 88, 49%).

MOG-IgG Serology

Antibody titers in serum were available in 31 patients with MOGAD (72%) with the remaining 12 MOGAD patients (28%) positive for MOG-IgG but without sufficient sample for end-titer determination. The median titer of MOG-IgG_1 was 1:100 (range 1:20–1:10,000), with 21 of 31 (68%) having high titers of ≥1:100. MOG-IgG in CSF was positive in 7 of 9 (78%) tested.

Comparison of Patients With Pediatric-Onset and Adult-Onset MOGAD With Tumefactive Lesions

When patients with MOGAD were divided according to the age at onset, seizures and sleepiness were more common in pediatric-onset patients. An MRI analysis revealed multiple concomitant tumefactive lesions occurred more frequently and lesions were larger in children, but other attributes were similar (eTables 1 and 2, links.lww.com/WNL/C597).

Figure 2 Long-term Outcomes of Patients With MOGAD With Tumefactive Lesions

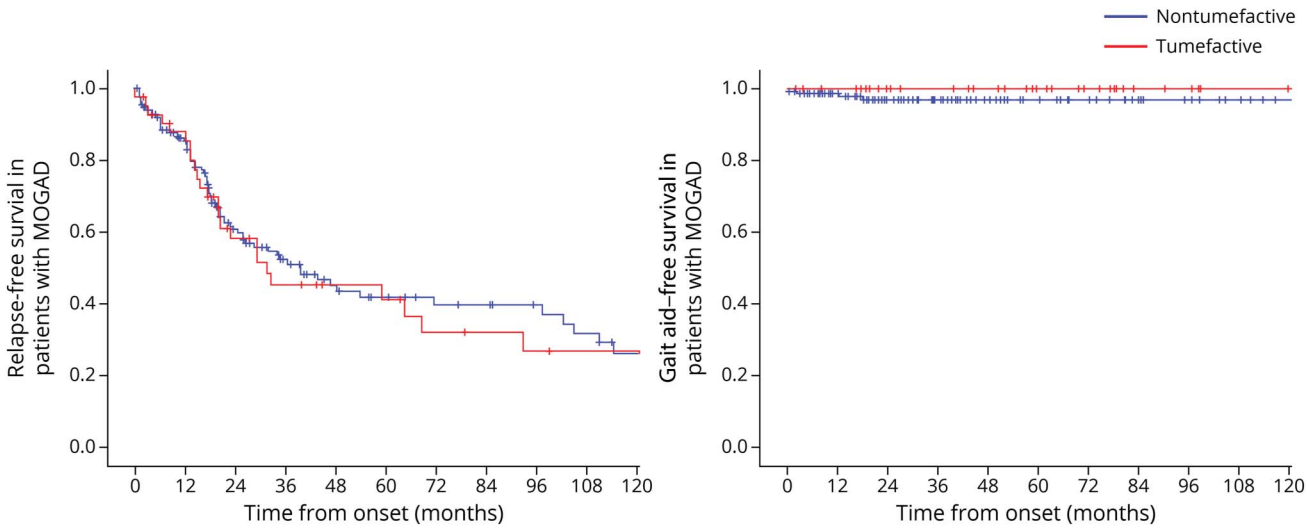

Kaplan-Meier curves of survival probability estimates of not developing relapse or reaching the EDSS disability milestone of 6 in patients with MOGAD up to 120 months from disease onset, according to the presence of tumefactive lesions. EDSS = Expanded Disability Status Scale; IgG = immunoglobulin G; MOGAD = myelin oligodendrocyte glycoprotein-IgG–associated disease.

Long-term Prognosis of Patients With MOGAD With Tumefactive Lesions

The median (interquartile range) duration of the clinical follow-up was 63 months (25–97) in patients with tumefactive MOGAD and 35 months (18–83) in those with nontumefactive MOGAD ($p = 0.046$). A gait aid was required in 5 of 151 patients with nontumefactive MOGAD (3%) and 1 of 43 patients with tumefactive MOGAD (2%, $p > 0.99$) at the last follow-up after over 282 months of disease duration. Deaths were also similarly rare in the 2 groups, occurring in 2 patients with nontumefactive MOGAD (1%) and 1 patient with tumefactive MOGAD (2%) ($p = 0.53$) at the last follow-up. The presence of tumefactive lesions was not associated with a higher risk of relapses (aHR 0.91, 95% CI 0.57–1.45, $p = 0.69$), need for gait aid (aHR 1.00, 95% CI 0.11–8.98, $p > 0.99$), or death (aHR 0.17, 95% CI 0.00–5.14, $p = 0.31$). The Kaplan-Meier curves estimating the cumulative risk of relapses and disability over 10 years of disease duration are shown in Figure 2.

Comparison of Frequency of Lesions and Patient Demographics, Clinical, and CSF Characteristics Between MOGAD, AQP4+NMOSD, and MS

We compared 43 patients with MOGAD with tumefactive lesions with 49 patients with MS and 16 patients with AQP4+NMOSD (Table 1). The frequency of tumefactive lesions in patients with MOGAD (43 of 194, 22%, see above) was higher than that observed in patients with AQP4+NMOSD (16 of 359, 5%, $p < 0.001$), but our methodology did not allow comparison with the frequency of tumefactive lesions in patients with MS. Patients with MOGAD were younger and more frequently had somnolence and headache, while aphasia was more suggestive of MS (Table 1). CSF oligoclonal bands were most frequent in MS while greater elevations in the CSF white blood cell count were noted in MOGAD than in MS (Table 1). Brain biopsies were rarely undertaken and did not reveal alternative etiologies. The complete details of the comparison of the demographic, clinical, and CSF features of the study population between these groups are summarized in Table 1.

Comparison of the Number of Brain Lesions and the Number of Tumefactive Brain Lesions

Patients with MOGAD had a lower median number of brain T2-hyperintense and gadolinium-enhancing lesions compared with those with MS, but similar to those with AQP4+NMOSD (Table 2). Comparison of lesion frequency including how many had multiple tumefactive lesions are summarized in Table 2.

Before the development of tumefactive brain lesions, an MRI with negative results was observed in 1 patient with MOGAD at 11 days from symptom onset and in 2 patients with MS, both at 5 days from onset. None of the patients with AQP4+NMOSD showed negative results for MRI while symptomatic.

Comparison of MRI Features of the Tumefactive Index Lesion

Overall, we evaluated 481 MRI scans of which 108 were acquired during the first tumefactive lesion attack and 373 acquired at follow-up (Table 2). The location, characteristics, and resolution of the index lesions are compared in Table 2. The MRI features of tumefactive lesions in the 3 diseases with key elements for the differential diagnosis are shown in Figure 3.

Table 1 Demographic, Clinical, and CSF Attributes of Tumefactive Demyelination Across the 3 Groups

	MOGAD (n = 43)	MS (n = 49)	MOGAD vs MS *p* value	AQP4+NMOSD (n = 16)	MOGAD vs AQP4+NMOSD *p* value
Age, y	21 (8–37)	36 (23–44)	**0.003**	40 (22–48)	**0.02**
Females	23 (54)	31 (63)	0.34	16 (100)	**<0.001**[a]
Pediatric onset	21 (49)	10 (20)	**0.004**	4 (25)	0.14[a]
Disease duration before initial tumefactive lesion detection, d	24 (11–195)	38 (11–640)	0.39	699 (15–2,272)	0.07
Tumefactive at onset	26 (61)	26 (53)	0.48	6 (38)	0.12
Tumefactive attack severity					
EDSS at nadir	3.5 (2.0–4.0)	3.0 (2.5–4.5)	0.57	4.0 (3.5–7.5)	0.11
ICU admission	3 (7)	2 (4)	0.66[a]	4 (25)	0.08[a]
Mechanical ventilation	2 (5)	0 (0)	0.22[a]	1 (6)	>0.99[a]
Clinical features					
Asymptomatic	4 (9)	6 (12)	0.65	3 (19)	0.28[a]
Symptoms/signs referable to brainstem or cerebellum	12 (28)	14 (29)	0.94	3 (19)	0.74[a]
Hemiparesis/monoparesis/quadriparesis	5 (12)	11 (22)	0.17	3 (19)	0.48[a]
Aphasia	1 (2)	10 (20)	**0.009**[a]	1 (6)	0.47[a]
Seizures	4 (9)	6 (12)	0.75[a]	2 (13)	0.66[a]
Somnolence	12 (28)	2 (4)	**0.003**[a]	0 (0)	**0.02**[a]
Vomiting or nausea	12 (28)	6 (12)	0.06	4 (25)	>0.99[a]
Headache	18 (42)	10 (20)	**0.03**	2 (13)	0.06[a]
Concomitant involvement of other CNS sites					
Optic neuritis	8 (19)	3 (6)	0.11[a]	0 (0)	0.09[a]
Myelitis	16 (37)	9 (18)	**0.04**	5 (31)	0.76
CSF findings					
Positive oligoclonal bands[b]	2 of 37 (5)	30 of 43 (70)	**<0.001**[a]	1 of 10 (10)	0.52[a]
White blood cell count, cells/μL[c]	33 (0–890)	6 (0–84)	**<0.001**	7 (0–188)	0.23
Elevated white blood cells[d]	32 of 40 (80)	18 of 34 (53)	**0.01**	6 of 9 (67)	0.39
Protein, mg/dL[c]	52 (13–126)	40 (17–160)	0.10	47 (26–251)	0.47
Glucose, mg/dL[c]	56 (38–87)	59 (44–96)	0.16	57 (39–93)	0.66
Brain biopsy	4 (9)	4 (8)	>0.99[a]	1 (6)	>0.99[a]

Abbreviations: AQP4+NMOSD = aquaporin-4-IgG–positive neuromyelitis optica spectrum disorders; d = days; EDSS = Expanded Disability Status Scale; ICU = intensive care unit; IgG = immunoglobulin G; MOGAD = myelin oligodendrocyte glycoprotein-IgG–associated disease; MS = multiple sclerosis; y = years.
Unless otherwise specified, quantitative variables are presented as median (interquartile range), and *p* values refer to the 2-way Kruskal Wallis test, while categorical variables are reported as n (%), and *p* values refer to the Pearson χ^2 test.
[a] The Fisher exact test.
[b] Oligoclonal bands were tested during the index clinical event in 21 of 37 patients with MOGAD (57%), 29 of 43 patients with MS (67%), and 4 of 10 patients with AQP4+NMOSD (40%).
[c] Data reported as median (range).
[d] White blood cell count >5 cells/μL.
Bold values are significant at $p < 0.05$.

Index Lesion Location

Compared with patients with MS, patients with MOGAD had a higher frequency of infratentorial tumefactive lesions, while periventricular and other white matter hemispheric lesions were less frequent. The localization of the index lesion in the deep gray matter (23%), corticospinal tract (14%), and corpus callosum (5%) was noted in MOGAD and AQP4+NMOSD (19%, 31%, and 19%, respectively), but not in MS.

Table 2 Comparison of MRI Features of Tumefactive Demyelination Across the 3 Groups

	MOGAD (n = 43)[a]	MS (n = 49)[a]	MOGAD vs MS *p* value	AQP4+NMOSD (n = 16)[a]	MOGAD vs AQP4+ NMOSD *p* value
Time from symptom onset, d	15 (7–21)	12 (5–29)	0.77	9 (3–15)	0.09
Total number of T2-hyperintense lesions	5 (3–14)	10 (5–27)	**0.008**	3.5 (2–10)	0.29
Total number of enhancing lesions	1 (0–2)	3 (1–6)	**<0.001**	1 (0–2)	0.78
Concomitant multiple tumefactive lesions	17 (40)	20 (41)	0.90	4 (25)	0.37[b]
Total number of concomitant tumefactive lesions	1 (1–2)	1 (1–2)	0.91	1 (1–2)	0.32
Diameters of the index lesion					
Longitudinal, cm	2.8 (2.3–3.3)	3.0 (2.4–4.5)	0.22	3.5 (2.5–4.1)	0.13
Cross-sectional, cm	1.7 (1.2–2.2)	2.3 (1.7–2.9)	**<0.001**	1.7 (1.3–2.2)	0.57
Location of the index lesion					
Infratentorial[c]	18 (42)	5 (10)	**<0.001**	5 (31)	0.57[b]
Deep gray matter	10 (23)	0 (0)	**<0.001**[b]	3 (19)	>0.99[b]
Periventricular[d]	4 (9)	23 (47)	**<0.001**[b]	4 (25)	0.19[b]
Corticospinal tract[e]	6 (14)	0 (0)	**0.009**[b]	5 (31)	0.15[b]
Corpus callosum	2 (5)	0 (0)	0.22[b]	3 (19)	0.12[b]
Hemispheric	8 (19)	21 (43)	**0.012**	1 (6)	0.42[b]
Other locations[f]	1 (2)	0 (0)	0.47[b]	0 (0)	>0.99[b]
Index lesion characteristics					
Mass effect	12 (28)	10 (20)	0.40	6 (38)	0.48
Baló-like	1 (2)	13 (27)	**0.001**[b]	0 (0)	>0.99[b]
Cystic component	2 (5)	20 (41)	**<0.001**[b]	1 (6)	>0.99[b]
Poorly demarcated borders	30 (70)	11 (22)	**<0.001**	8 (50)	0.16
T2-hypointense rim	1 (2)	32 (65)	**<0.001**[b]	0 (0)	>0.99[b]
T1-hypointensity	21 (49)	46 (94)	**<0.001**	12 (75)	0.07
DWI restriction	11 of 42 (26)	48 (98)	**<0.001**	10 of 15 (67)	**0.005**
Arc peripheral DWI restriction	2 of 42 (5)	38 (78)	**<0.001**[b]	1 of 15 (7)	>0.99[b]
Contrast enhancement	23 (54)	43 of 47 (92)	**<0.001**	8 (50)	0.81
Ring[g]	1 (2)	18 of 47 (38)	**<0.001**[b]	1 (6)	0.47[b]
Cloud-like	3 (7)	3 of 47 (6)	>0.99[b]	2 (13)	0.61[b]
Concomitant MRI features of other CNS sites					
Optic nerve					
Optic nerve enhancement	6 of 15 (40)	2 of 9 (22)	0.66[b]	0 of 4 (0)	0.26[b]
Bilateral optic nerve enhancement	2 of 15 (13)	0 of 9 (0)	0.51[b]	0 of 4 (0)	>0.99[b]
Optic nerve enhancement involving >50% of length	4 of 15 (27)	1 of 9 (11)	0.62[b]	0 of 4 (0)	0.53[b]
Optic nerve sheath enhancement	3 of 15 (20)	0 of 9 (0)	0.27[b]	0 of 4 (0)	>0.99[b]
Spinal cord					
Presence of T2-hyperintense spinal cord lesion	16 of 27 (59)	21 of 39 (54)	0.66	8 of 10 (80)	0.24

Continued

Table 2 Comparison of MRI Features of Tumefactive Demyelination Across the 3 Groups *(continued)*

	MOGAD (n = 43)[a]	MS (n = 49)[a]	MOGAD vs MS *p* value	AQP4+NMOSD (n = 16)[a]	MOGAD vs AQP4+ NMOSD *p* value
Presence of T2-hyperintense spinal cord lesion in the conus	11 of 27 (41)	3 of 33 (9)	**0.006**[b]	1 of 9 (11)	0.22[b]
Central lesions	9 of 16 (56)	2 of 21 (10)	**0.003**[b]	3 of 8 (38)	0.67[b]
Peripheral lesions	0 of 16 (0)	14 of 21 (67)	**<0.001**[b]	0 of 8 (0)	—
Mixed central and peripheral lesions	7 of 16 (44)	5 of 21 (24)	0.20	5 of 8 (63)	0.39
Longitudinally extensive T2 hyperintense spinal cord lesion	13 of 27 (48)	3 of 39 (8)	**<0.001**[b]	8 of 10 (80)	0.08
Spinal cord enhancement	12 of 27 (44)	11 of 39 (28)	0.17	6 of 10 (60)	0.40
Follow-up evolution of the index lesion					
Time from baseline to the first follow-up MRI scan, d	195 (141–518)	189 (130–266)	0.25	369 (237–2,135)	**0.02**
Complete resolution on T2-images at the first follow-up MRI scan	19 of 35 (54)	0 of 42 (0)	**<0.001**[b]	0 of 14 (0)	**<0.001**[b]
Complete resolution on T1-images at the first follow-up MRI scan	24 of 35 (69)	6 of 42 (14)	**<0.001**	4 of 14 (29)	**0.02**[b]
Time from baseline to the last follow-up MRI scan, m	35 (20–75)	25 (10–61)	0.18	24 (8–72)	0.45
Complete resolution on T2-images at the last follow-up MRI scan	23 of 35 (66)	0 of 42 (0)	**<0.001**[b]	2 of 14 (14)	**0.001**[b]
Complete resolution on T1-images at the last follow-up MRI scan	30 of 35 (86)	13 of 42 (31)	**<0.001**	5 of 14 (36)	**<0.001**

Abbreviations: AQP4+NMOSD = aquaporin-4-IgG–positive neuromyelitis optica spectrum disorders; cm = centimeters; d = days; DWI = diffusion-weighted imaging; IgG = immunoglobulin G; m = months; MOGAD = myelin oligodendrocyte glycoprotein-IgG–associated disease; MS = multiple sclerosis.
Unless otherwise specified, quantitative variables are presented as median (interquartile range), and *p* values refer to the 2-way Kruskal Wallis test, while categorical variables are reported as n (%), and *p* values refer to the Pearson χ^2 test.
[a] All categorical values and percentages are out of this denominator unless specified.
[b] The Fisher exact test.
[c] Infratentorial lesions involved the following: (1) the middle cerebellar peduncle: MOGAD (n = 7, 16%), MS (n = 4, 8%), and AQP4+NMOSD (n = 1, 6%); (2) the medulla, pons, or midbrain: MOGAD (n = 11, 26%) and AQP4+NMOSD (n = 4, 25%, one of which extending to the middle cerebellar peduncle, hence also included above); (3) the cerebellum: MS (n = 1, 2%) and AQP4+NMOSD (n = 1, 6%).
[d] A periventricular lesion detected in a patient with AQP4+NMOSD also involved the splenium of the corpus callosum (arch bridge pattern, Figure 2).
[e] Tumefactive lesions in the corticospinal tract usually extended to contiguous structures such as the thalamus (5 MOGAD and 2 AQP4+NMOSD) and the midbrain (1 MOGAD and 1 AQP4+NMOSD).
[f] Hippocampus in 1 patient with MOGAD.
[g] Ring enhancement included the following: (1) closed ring enhancement: MOGAD (n = 1, 2%), MS (n = 6, 12.0%), and AQP4+NMOSD (n = 1, 6%) and (2) open ring enhancement: MS (n = 12, 24%).
Bold values are significant at $p < 0.05$.

Index Lesion Characteristics

Attributes of the index lesion favoring MS over MOGAD included the following: a T2-hypointense rim, T1-hypointensity, diffusion-weighted imaging (DWI) restriction (particularly when in an arc pattern), Baló-like appearance and a cystic component, and open or closed rings of enhancement. DWI restriction was also more common in patients with AQP4+NMOSD compared with patients with MOGAD. Mass effect did not differ between groups, and cloud-like enhancement was rare across all groups (Table 2).

Lesion Evolution

Follow-up MRIs were available in 35 of 43 patients with MOGAD (81%), 42 of 49 patients with MS (86%), and 14 of 16 patients with AQP4+NMOSD (88%). The median number (range) of scans per patient was 3 (1–12) for MOGAD, 3 (1–19) for MS, and 2 (1–9) for AQP4+NMOSD. It was similar between MOGAD and MS ($p = 0.58$), but lower in AQP4+NMOSD compared with that in MOGAD ($p = 0.03$). At the first follow-up, details regarding ongoing treatment were available for all but 2 patients with MOGAD. Of them, disease-modifying medications or oral steroids were administered to 14 of 33 patients with MOGAD (42%), 27 of 42 patients with MS (64%), and 11 of 14 (79%) patients with AQP4+NMOSD. In those off of oral steroids, the median (interquartile range) time to oral steroid discontinuation was 2.5 (2–8) months in MOGAD and 18 (1–38) months in AQP4+NMOSD, respectively.

A complete resolution of the index tumefactive lesions on T2-weighted images was observed in 19 of 35 (54%) patients with MOGAD, but not in the other groups (Table 2, Figure 3).

Figure 3 Examples of Tumefactive Brain Lesions and Relevant MRI Features for the Differential Diagnosis of Patients With MOGAD, MS, and AQP4+NMOSD

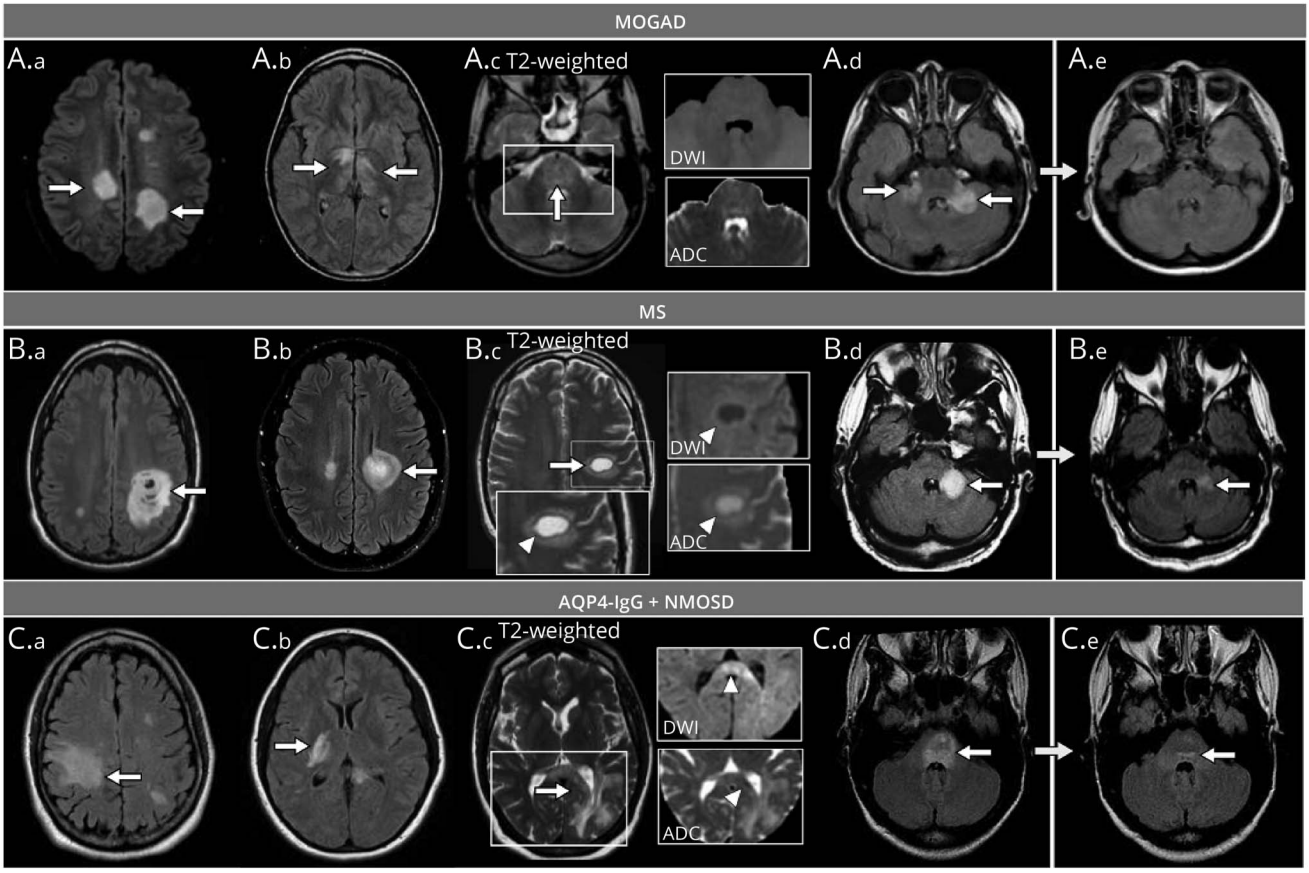

Unless otherwise specified, lesions are shown on axial T2-fluid-attenuated inversion recovery (T2-FLAIR). Tumefactive lesions are indicated by white arrows, while specific features are indicated by arrowheads. Panel A (MOGAD): tumefactive lesions in the bilateral hemispheric white matter (A.a, arrows); bilateral tumefactive lesions in the corticospinal tract and thalami (A.b, arrows); tumefactive lesion involving the entire pons (A.c, arrow) without evidence of T2-hypointense rim, diffusion restriction (i.e., no DWI hyperintensity), and no ADC map hypointensity (A.c); bilateral tumefactive lesions in the middle cerebellar peduncles (A.d, arrows), with complete resolution at follow-up MRI (A.e). Panel B (MS): Baló-like tumefactive lesions in the hemispheric white matter (B.a, arrow) and periventricular white matter (B.b, arrow); tumefactive lesion located in the hemispheric white matter, showing a complete T2-hypointense rim (arrowhead) with a corresponding ring of peripheral diffusion restriction, as indicated by the hyperintensity in DWI (arrowhead) and hypointensity on ADC map (arrowhead) (B.c); tumefactive lesion in the left middle cerebellar peduncle (B.d, arrow) undergoing volumetric reduction, but still present at follow-up MRI (B.e, arrow). Panel C (AQP4+NMOSD): tumefactive lesions in the hemispheric white matter (C.a, arrow), corticospinal tract (C.b, arrow); tumefactive periventricular lesion extensively involving the splenium of the corpus callosum in an "arch-bridge" pattern (C.c, arrow); the lesion does not show any T2-hypointense rim and is characterized by DWI hyperintensity of the splenium (arrowhead) with focal diffusion restriction (i.e., corresponding hypointensity on the ADC map, arrowhead); tumefactive lesion involving the entire pons (C.d, arrow), showing residual mild hyperintensity near the fourth ventricle (C.e, arrow). ADC = apparent diffusion coefficient map; AQP4+NMOSD = aquaporin-4-IgG–positive neuromyelitis optica spectrum disorders; DWI = diffusion-weighted images; IgG = immunoglobulin G; MOGAD = myelin oligodendrocyte glycoprotein-IgG–associated disease; MS = multiple sclerosis.

Residual T1-hypointensity on follow-up MRI was rare in MOGAD, but common with MS and AQP4+NMOSD. Similar results were observed at the last follow-up MRI scan.

Distinguishing MOGAD Tumefactive Lesions From Other Demyelinating Etiologies Using Clinical and MRI Features

Results of the univariable binary logistic regression models (Table 3) assessing associations between clinical or MRI variables and MOGAD diagnosis are reported in the eTable 3 (links.lww.com/WNL/C597).

To avoid separation, the following variables were merged, based on their similarity: (1) the presence of somnolence or headache; (2) concomitant involvement of other CNS sites (e.g., optic neuritis or myelitis); (3) lesion location in brain regions not found in patients with MS (deep gray matter, corticospinal tract, and corpus callosum; this feature was not included in the model MOGAD vs MS); (4) Baló-like or cystic component appearance; (5) a complete resolution on T2-weighted or T1-weighted images. A T2-hypointense rim was not encountered in AQP4+NMOSD, so this feature was not included in the model of MOGAD vs AQP4+NMOSD.

Because the availability of CSF samples, optic nerve MRI, and spinal cord MRI was limited, these variables were not included in the final model. However, the presence of positive oligoclonal bands favored MS, while CSF white blood cell elevation

Table 3 Multivariable Binary Logistic Regression Analysis Between Clinical/MRI Variables and MOGAD Diagnosis

	β (SE)	OR (95% CI)	*p* Value	Nagelkerke R^2	+ Complete resolution on T1- or T2-images
MOGAD vs other demyelinating disorders					
Somnolence or headache	1.5 (0.7)	4.51 (1.12–18.04)	0.03	0.67	0.73
T2-hypointense rim	−3.4 (1.4)	0.03 (0.00–0.49)	0.01		
T1-hypointensity	−1.7 (0.7)	0.19 (0.05–0.77)	0.02		
DWI restriction	−2.5 (0.6)	0.09 (0.03–0.29)	<0.001		
MOGAD vs MS					
Somnolence or headache	2.4 (1.3)	11.04 (0.82–148.41)	0.07	0.86	0.96
Periventricular lesions	−2.11 (1.1)	0.12 (0.01–1.07)	0.06		
T2-hypointense rim	−3.26 (1.5)	0.04 (0.00–0.80)	0.03		
DWI restriction	−2.90 (1.3)	0.06 (0.00–0.75)	0.03		
Arc peripheral DWI restriction	−3.13 (1.5)	0.04 (0.00–0.78)	0.03		
MOGAD vs AQP4+NMOSD					
Somnolence or headache	1.69 (0.9)	5.39 (1.01–28.78)	0.049	0.29	0.44
DWI restriction	−1.65 (0.7)	0.19 (0.05–0.73)	0.02		

Abbreviations: AQP4+NMOSD = aquaporin-4-IgG–positive neuromyelitis optica spectrum disorders; DWI = diffusion-weighted imaging; IgG = immunoglobulin G; MOGAD = myelin oligodendrocyte glycoprotein-IgG–associated disease; MS = multiple sclerosis.
Data are presented as β coefficient (SE) and odds ratio (95% CI).

and longitudinally extensive spinal cord lesions, especially if involving the conus and centrally located, were associated with MOGAD (eTable 3, links.lww.com/WNL/C597).

Independent predictors of MOGAD diagnosis over other demyelinating disorders were the presence of somnolence or headache and the absence of T2-hypointense rim, T1-hypointensity, or DWI restriction (Nagelkerke R^2 = 0.67).

The presence of somnolence or headache and the absence of periventricular location, T2-hypointense rim, and any type or arc peripheral DWI restriction supported MOGAD over MS (Nagelkerke R^2 = 0.86), while the presence of somnolence or headache and the absence of DWI restriction favored MOGAD over AQP4+NMOSD (Nagelkerke R^2 = 0.29).

When the complete resolution of the index tumefactive lesions on T2-weighted or T1-weighted images at the first follow-up MRI scan was included, the performance of all models improved in differentiating MOGAD from the other diseases (Table 3). We did not consider lesion resolution at the last follow-up MRI scan in our model because it would be less useful in the acute clinical setting.

Comparison of Subsequent Tumefactive Lesions

The rate of subsequent tumefactive lesions across the 3 groups was similar: 6 of 35 patients with MOGAD (17%), 5 of 42 patients with MS (12%, *p* vs MOGAD = 0.74), and 2 of 14 patients with AQP4+NMOSD (14%, *p* vs MOGAD >0.99) (Table 4). In total, we observed 20 recurrent tumefactive attacks (11 in MOGAD, 7 in MS, and 2 in AQP4+NMOSD), the features of the subsequent tumefactive lesions when compared with those of the baseline lesions are summarized in Table 4 and examples are shown in eFigure 1 (links.lww.com/WNL/C597).

Discussion

In this study, we found tumefactive lesions were frequent in MOGAD but did not convey an increased risk of relapse or worse outcome. The clinical manifestations, MRI, and CSF features of patients with MOGAD with tumefactive lesions had many differences from those of patients with MS but were similar to those of patients with AQP4+NMOSD.

Tumefactive lesions occurred in 22% of patients with MOGAD, which was greater than that in patients with AQP4+NMOSD (5% in this study and 0%–3.4% in prior studies).[9,10] Although our search criteria precluded the analysis of the frequency of tumefactive demyelination in MS, a prior population-based study at our facility reported it in 1.9% of patients with MS,[9] and in studies from other centers, it has ranged from 0.1% to 2.1% of patients with MS.[28,29] Notably, tumefactive lesions were detected in almost 50% of patients with MOGAD with brain attacks, and thus tumefactive brain lesions account for a far higher proportion of brain lesions in MOGAD than in MS and AQP4+NMOSD. Therefore, in the

Table 4 MRI Features of Subsequent Tumefactive Demyelination Across the 3 Groups

	Subsequent tumefactive lesions			Proportion of subsequent tumefactive lesions with the feature present also at first tumefactive attack		
	MOGAD (n = 11)	MS (n = 7)	AQP4+NMOSD (n = 2)	MOGAD	MS	AQP4+NMOSD
Location of index lesion						
Infratentorial	4 (36)	2 (29)	2 (100)	1 of 4 (25)	1 of 2 (50)	1 of 2 (50)
Deep gray matter	1 (9)	0 (0)	0 (0)	**1 of 1 (100)**	Not applicable	Not applicable
Periventricular	1 (9)	2 (29)	0 (0)	0 of 1 (0)	1 of 2 (50)	Not applicable
Corticospinal tract[a]	2 (18)	0 (0)	1 (50)	0 of 2 (0)	Not applicable	**1 of 1 (100)**
Corpus callosum	1 (9)	0 (0)	0 (0)	0 of 1 (0)	Not applicable	Not applicable
Hemispheric	4 (36)	3 (43)	0 (0)	0 of 4 (0)	**3 of 3 (100)**	Not applicable
Index lesion MRI characteristics						
Mass effect	1 (9)	5 (71)	1 (50)	0 of 1 (0)	2 of 5 (40)	**1 of 1 (100)**
Baló-like	0 (0)	0 (0)	0 (0)	Not applicable	Not applicable	Not applicable
Cystic component	0 (0)	2 (29)	0 (0)	Not applicable	**2 of 2 (100)**	Not applicable
Poorly demarcated borders	10 (91)	2 (29)	1 (50)	**8 of 10 (80)**	1 of 2 (50)	1 of 2 (50)
T2 hypointense rim	0 (0)	5 (71)	0 (0)	Not applicable	**4 of 5 (80)**	Not applicable
T1-hypointensity	9 (82)	7 (100)	2 (100)	**8 of 9 (89)**	**6 of 7 (86)**	1 of 2 (50)
DWI restriction	1 (9)	6 (86)	2 (100)	0 of 1 (0)	**6 of 6 (100)**	**2 of 2 (100)**
Arc peripheral DWI restriction	0 (0)	5 (71)	0 (0)	Not applicable	2 of 5 (40)	Not applicable
Contrast enhancement	9 (82)	6 (86)	2 (100)	6 of 9 (67)	**3 of 3**[b] **(100)**	0 of 2 (0)
Ring	0 (0)	3 (43)	0 (0)	Not applicable	**1 of 1**[b] **(100)**	Not applicable
Cloud-like	3 (27)	0 (0)	1 (50)	1 of 3 (33)	Not applicable	0 of 1 (0)
Follow-up evolution of the index lesion						
Complete resolution on T2-images at the first follow-up MRI scan	5 of 10 (50)	0 of 6 (0)	0 of 1 (0)	**4 of 5 (80)**	Not applicable	Not applicable
Complete resolution on T1-images at the first follow-up MRI scan	6 of 10 (60)	0 of 6 (0)	0 of 1 (0)	**6 of 6 (100)**	Not applicable	Not applicable
Complete resolution on T2-images at the last follow-up MRI scan	5 of 10 (50)	0 of 6 (0)	0 of 1 (0)	**4 of 5 (80)**	Not applicable	Not applicable
Complete resolution on T1-images at the last follow-up MRI scan	7 of 10 (70)	0 of 6 (0)	0 of 1 (0)	**7 of 7 (100)**	Not applicable	Not applicable

Abbreviations: AQP4+NMOSD = aquaporin-4-IgG–positive neuromyelitis optica spectrum disorders; DWI = diffusion-weighted imaging; IgG = immunoglobulin G; MOGAD = myelin oligodendrocyte glycoprotein-IgG–associated disease; MS = multiple sclerosis.
Data refer to the index lesion of each tumefactive attack. To improve readability, if the proportion of subsequent tumefactive lesions with a certain feature already present at the first tumefactive attack was at least 80%, this was highlighted in bold.
[a] Tumefactive lesions in the corticospinal tract usually extended to contiguous structures such as the thalamus (1 MOGAD) and the midbrain (1 MOGAD and 1 AQP4+NMOSD).
[b] Gadolinium not administered during the first tumefactive attack in a patient with multiple tumefactive attacks.

presence of an inflammatory-appearing tumefactive lesion, MOG-IgG testing should be considered, although we must keep in mind that the overall incidence of MS far exceeds MOGAD. Indeed, given MOGAD brain MRI changes can take time to develop (noted in 1 patient in this study) or be subtle (e.g., cerebral cortical encephalitis), MOG-IgG testing early on can be especially helpful when the initial radiologic picture is uncertain. Tumefactive lesions in MOGAD sometimes needed intensive care unit admission and ventilatory support, as previously reported.[30] However, despite the severe clinical features acutely, our study shows that in MOGAD, the presence of tumefactive demyelination was not associated with a greater risk of relapse or long-term physical disability.[31]

Regarding clinical presentation, features of encephalopathy, especially somnolence, were more common among patients with MOGAD than among those with MS and AQP4+NMOSD, in line with the higher prevalence of acute disseminated encephalomyelitis phenotype observed in this disease, particularly during childhood.[32] In our cohort, the clinical presentation of tumefactive demyelination of patients with MS was polysymptomatic in approximately one-third of the patients. Although not standard in typical MS, similar findings were found in other cohorts of tumefactive MS[4,33] and may reflect the high degree of inflammatory activity spreading to other regions such as the optic nerve or spinal cord. It is also notable that tumefactive demyelination usually occurred in the first 2 years from onset, earlier in patients with MOGAD and MS than in those with AQP4+NMOSD, although a small proportion developed attacks with tumefactive lesions later on. Possible explanations for this include the early use of more effective disease-modifying treatments in those with aggressive inflammatory activity at onset and the first attack being recognized to be the most severe in MOGAD.[34]

In our tumefactive MS cohort, the frequency of oligoclonal bands (70%) was slightly lower than that typically observed in patients with MS (approximately 88%),[35] but it was still useful in discriminating from MOGAD. The reasons for the lower frequency of CSF oligoclonal bands in our tumefactive MS cohort is uncertain but in line with previous studies on tumefactive MS (52%–66%).[9,36] The presence of other clinical and radiologic features consistent with MS, pathologic confirmation of demyelination in some, and absence of alternative diagnoses in longitudinal follow-up, further supported an MS diagnosis in these cases.

In our cohort, the differentiation between tumefactive lesions due to MS rather than MOGAD was feasible with conventional MRI sequences. Compared with MS, tumefactive lesions in MOGAD were preferentially located in the posterior fossa and deep gray matter, while were less frequently found in the periventricular and hemispheric white matter. Infratentorial involvement is considered a well-established radiologic finding in MOGAD, where lesions can have poorly demarcated borders (i.e., fluffy appearance)[21] and extensively involve the middle cerebellar peduncles or, less frequently, the medulla, pons, and midbrain.[11] Conversely, MS lesions have a tropism for the deep medullary veins running perpendicular to the outline of the ventricular system.[21]

We identified a number of MRI features that were frequent in MS and rarely observed in MOGAD, including the presence of a T2-hypointense rim, DWI restriction (especially when arc-shaped), ring enhancement, and T1-hypointensity. A T2-hypointense rim has been observed in 45% of tumefactive lesions with pathologic evidence of confluent inflammatory demyelination consistent with MS[4] and in around 9% of patients with MS, irrespective of lesion dimension.[22] Studies also suggest a certain degree of association between the hypointense rim and the presence of ring enhancement, although both can occur in isolation as well.[4,22] Prior pathology studies revealed that an iron-rich macrophage layer surrounding pattern I and II active demyelinating lesions represents the pathologic correlate of the T2-hypointense rim.[37,38] In addition, although macrophage densities are similar across immunopatterns of early active demyelinating lesions, macrophages in pattern II lesions are characterized by a higher expression of the heavy subunit of the iron-storage protein ferritin and by internal iron accumulation.[39] The colocalization of iron with the peripheral border of macrophages could therefore locally reduce the T2-relaxation time, leading to the identification of a corresponding area of T2-hypointense signal.[40]

Discriminating between MOGAD and AQP4+NMOSD was more challenging, and a large overlap of clinical and radiologic manifestations was noticed, in line with previous findings.[25,32] However, lesions in MOGAD showed a lower rate of restricted diffusion, which was the only significant MRI discriminant from AQP4+NMOSD at baseline. In agreement with the relatively benign course of MOGAD, a previous study suggested that the presence of restricted diffusion, likely due to altered fiber tract organization or cellular infiltrates, might reflect a more severe degree of tissue damage.[12] A lower degree of tissue damage might also explain the numerically lower rate of T1-hypointensity[38] in MOGAD, whose absence favored MOGAD diagnosis over other demyelinating disorders.

This also aligns with the observation of a complete resolution of tumefactive T2-hyperintense lesions in approximately 54% of patients with MOGAD at the first follow-up MRI, as opposed to none of the patients with AQP4+NMOSD and MS. Similar results were found in other studies, showing lesion resolution in 72% of cases with MOGAD, but uncommon (5%–24%) lesion resolution in cases with AQP4+NMOSD or MS.[41,42] When we included this feature as an explanatory variable for MOGAD identification, all model performances improved, especially when considering the differential diagnosis with AQP4+NMOSD, emphasizing its clinical usefulness when available. Nonetheless, when evaluating tumefactive lesions at onset, the information on lesion resolution will not be available, and this makes radiologic discrimination between these diseases more challenging at the initial presentation. In patients with subsequent tumefactive attacks, the presence of those features already identified as the most relevant for differential diagnosis (i.e., T2-hypointense rim, DWI restriction, T1-hypointensity, and lesion resolution) were generally concordant in different episodes, strengthening their utility in clinical practice.

Regarding limitations, we acknowledge the retrospective design, the relatively small sample size (especially for the

AQP4+NMOSD cohort), and the lack of biopsy characterization of all lesions. However, because biopsy is invasive with the potential for neurologic morbidity, it is usually performed only in cases of greatest diagnostic uncertainty with atypical elements, and inclusion of all tumefactive cases regardless of biopsy may better reflect the spectrum of tumefactive lesions encountered in clinical practice. In addition, in those biopsied from this study, we did not focus on their pathology features, which we have reported in detail previously.[37,43-45] The absence of a noninflammatory control group is an additional limitation, but discriminators from alternative etiologies of large lesions can still be extrapolated from our study. For example, the presence of mass effect and avid contrast enhancement would favor tumor over MOGAD,[33] while ring enhancement and a core of restricted diffusion would favor abscesses over MOGAD.[12] In addition, caution should be applied to the interpretation of longitudinal data (i.e., the rate of lesion resolution and recurrent tumefactive lesions) because MRI timing and frequency was not standardized, and different scanners were used at onset and follow-up, as expected in a clinical setting.

However, all this considered, our study provides several clinical and MRI features (i.e., the presence of somnolence and the absence of periventricular location, T2-hypointense rim, T1-hypointensity, and any shape or arc peripheral DWI restriction), which might assist in the correct identification of tumefactive lesions due to MOGAD rather than MS and, to a lesser extent, AQP4+NMOSD. The recognition of different MRI patterns of inflammatory tumefactive demyelination emphasizes the distinct pathophysiology of each disorder and might contrast with the concept of pseudotumoral demyelination as a separate entity.[46] Future studies exploring the pathologic correlates of tumefactive lesions in different demyelinating diseases will help clarify this. In addition, future lines of research could assess double-seronegative NMOSD, which are a more heterogeneous group of disorders and not a focus of this study. Finally, this study furtherly underlines the importance of follow-up MRI when the diagnosis is uncertain because the complete resolution of lesions was confirmed, once again, as a reliable hallmark of MOGAD.

Study Funding

This study was funded by an RO1 from the National Institute of Neurological Disorders and Stroke (R01NS113828).

Disclosure

L. Cacciaguerra received speaker and consultant honoraria from ACCMED, Roche, BMS Celgene, and Sanofi. P. Morris reports no disclosures. W.O. Tobin has received research funding from Mallinckrodt Inc., the Mayo Clinic Center for Multiple Sclerosis and Autoimmune Neurology, and the NIH (grant R01NS113803 and R01NS121928) outside the submitted work; he has received honoraria from Neurology Live and has coedited *Mayo Clinic Cases in Neuroimmunology*. J.J. Chen served as consultant for Roche and UCB. S.A. Banks, P. Elsbernd, and V. Redenbaugh report no disclosures. J.-M. Tillema is associate editor for the *Journal of Child Neurology*. F. Montini and E. Sechi report no disclosures. A.S. Lopez-Chiriboga has served on advisory boards for Genentech and Horizon Therapeutics. N.L. Zalewski and Y. Guo report no disclosures. M. Assunta Rocca received speaker honoraria from Bayer, Biogen, Bristol Myers Squibb, Celgene, Genzyme, Merck Serono, Novartis, Roche, and Teva and receives research support from the MS Society of Canada and Fondazione Italiana Sclerosi Multipla. M. Filippi is editor-in-chief of the *Journal of Neurology*, associate editor of *Human Brain Mapping*, associate editor of *Radiology*, and associate editor of *Neurological Sciences*; received compensation for consulting services and/or speaking activities from Almiral, Alexion, Bayer, Biogen, Celgene, Eli Lilly, Genzyme, Merck-Serono, Novartis, Roche, Sanofi, Takeda, and Teva Pharmaceutical Industries; and receives research support from Biogen Idec, Merck-Serono, Novartis, Roche, Teva Pharmaceutical Industries, Italian Ministry of Health, Fondazione Italiana Sclerosi Multipla, and ARiSLA (Fondazione Italiana di Ricerca per la SLA). S.J. Pittock reports grants, personal fees, and nonfinancial support from Alexion Pharmaceuticals, Inc.; grants, personal fees, nonfinancial support, and other support from MedImmune, Inc./Viela Bio, Inc.; and personal fees for consulting from Genentech/Roche; he has a patent, patent # 8,889,102 (application #12-678350, Neuromyelitis Optica Autoantibodies as a Marker for Neoplasia)—issued and a patent, patent # 9,891,219B2 (application #12-573942, Methods for Treating Neuromyelitis Optica [NMO] by Administration of Eculizumab to an individual that is Aquaporin-4 [AQP4]–IgG Autoantibody positive)—issued. C.F. Lucchinetti received grants from the National Institute of Health, National Multiple Sclerosis Society, National Institute of Neurological Disorders and Stroke, Kingsland Foundation, Biogen Idec. E.P. Flanagan has served on advisory boards for Alexion, Genentech, and Horizon Therapeutics, has received speaker honoraria from Pharmacy Times, and received royalties from UpToDate. Dr. Flanagan was a site primary investigator in a randomized clinical trial on Inebilizumab in neuromyelitis optica spectrum disorder run by Medimmune/Viela-Bio/Horizon Therapeutics, has received funding from the NIH (R01NS113828), and is a member of the medical advisory board of the MOG project. Dr. Flanagan is an editorial board member of the *Journal of the Neurological Sciences* and *Neuroimmunology Reports*, and a patent has been submitted on DACH1-IgG as a biomarker of paraneoplastic autoimmunity. Go to Neurology.org/N for full disclosures.

Publication History

Received by *Neurology* May 26, 2022. Accepted in final form December 2, 2022. Submitted and externally peer reviewed. The handling editor was Deputy Editor Olga Ciccarelli, MD, PhD, FRCP.

Appendix Authors

Name	Location	Contribution
Laura Cacciaguerra, MD	Department of Neurology and Mayo Clinic Center for Multiple Sclerosis and Autoimmune Neurology, Mayo Clinic, Rochester, MN; Vita-Salute San Raffaele University; Neuroimaging Research Unit, Division of Neuroscience, IRCCS San Raffaele Scientific Institute, Milan, Italy	Drafting/revision of the article for content, including medical writing for content; major role in the acquisition of data; and analysis or interpretation of data
Pearse Morris, MBBCh	Department of Radiology, Mayo Clinic, Rochester, MN	Drafting/revision of the article for content, including medical writing for content; major role in the acquisition of data; and analysis or interpretation of data
W. Oliver Tobin, MBBCh, PhD	Department of Neurology and Mayo Clinic Center for Multiple Sclerosis and Autoimmune Neurology, Mayo Clinic, Rochester, MN	Drafting/revision of the article for content, including medical writing for content; major role in the acquisition of data; and analysis or interpretation of data
John J. Chen, MD, PhD	Department of Neurology and Mayo Clinic Center for Multiple Sclerosis and Autoimmune Neurology, Department of Ophthalmology, Mayo Clinic, Rochester, MN	Drafting/revision of the article for content, including medical writing for content; major role in the acquisition of data; and analysis or interpretation of data
Samantha A. Banks, MD	Department of Neurology and Mayo Clinic Center for Multiple Sclerosis and Autoimmune Neurology, Mayo Clinic, Rochester, MN	Major role in the acquisition of data; analysis or interpretation of data
Paul Elsbernd, MD	Department of Neurology, San Antonio Military Medical Center, Fort Sam Houston, TX	Major role in the acquisition of data; analysis or interpretation of data
Vyanka Redenbaugh, MD	Department of Neurology and Mayo Clinic Center for Multiple Sclerosis and Autoimmune Neurology, Mayo Clinic, Rochester, MN	Major role in the acquisition of data; analysis or interpretation of data
Jan-Mendelt Tillema, MD	Department of Neurology and Mayo Clinic Center for Multiple Sclerosis and Autoimmune Neurology, Mayo Clinic, Rochester, MN	Major role in the acquisition of data; analysis or interpretation of data
Federico Montini, MD	Vita-Salute San Raffaele University; Neurology Unit, IRCCS San Raffaele Scientific Institute, Milan, Italy	Drafting/revision of the article for content, including medical writing for content
Elia Sechi, MD	Department of Medical, Surgical and Experimental Sciences, University of Sassari, Italy	Drafting/revision of the article for content, including medical writing for content
A. Sebastian Lopez-Chiriboga, MD	Department of Neurology, Mayo Clinic, Jacksonville, FL	Major role in the acquisition of data; analysis or interpretation of data
Nicholas Zalewski, MD	Department of Neurology, Mayo Clinic, Scottsdale, AZ	Major role in the acquisition of data; analysis or interpretation of data
Yong Guo, MD, PhD	Department of Neurology and Mayo Clinic Center for Multiple Sclerosis and Autoimmune Neurology, Mayo Clinic, Rochester, MN	Major role in the acquisition of data; analysis or interpretation of data
Maria A. Rocca, MD	Vita-Salute San Raffaele University; Neuroimaging Research Unit, Division of Neuroscience, IRCCS San Raffaele Scientific Institute; Neurology Unit, IRCCS San Raffaele Scientific Institute, Milan, Italy	Drafting/revision of the article for content, including medical writing for content
Massimo Filippi, MD	Vita-Salute San Raffaele University; Neuroimaging Research Unit, Division of Neuroscience, IRCCS San Raffaele Scientific Institute; Neurology Unit, IRCCS San Raffaele Scientific Institute; Neurorehabilitation Unit, IRCCS San Raffaele Scientific Institute; Neurophysiology Service, IRCCS San Raffaele Scientific Institute, Milan, Italy	Drafting/revision of the article for content, including medical writing for content
Sean J. Pittock, MD	Department of Neurology and Mayo Clinic Center for Multiple Sclerosis and Autoimmune Neurology, Laboratory Medicine and Pathology, Mayo Clinic, Rochester, MN	Drafting/revision of the article for content, including medical writing for content; major role in the acquisition of data; and analysis or interpretation of data
Claudia F. Lucchinetti, MD	Department of Neurology and Mayo Clinic Center for Multiple Sclerosis and Autoimmune Neurology, Mayo Clinic, Rochester, MN	Drafting/revision of the article for content, including medical writing for content; major role in the acquisition of data; and analysis or interpretation of data
Eoin P. Flanagan, MBBCh	Department of Neurology and Mayo Clinic Center for Multiple Sclerosis and Autoimmune Neurology, Laboratory Medicine and Pathology, Mayo Clinic, Rochester, MN	Drafting/revision of the article for content, including medical writing for content; major role in the acquisition of data; study concept or design; and analysis or interpretation of data

References

1. Reindl M, Waters P. Myelin oligodendrocyte glycoprotein antibodies in neurological disease. *Nat Rev Neurol*. 2019;15(2):89-102. doi:10.1038/s41582-018-0112-x.
2. Jarius S, Paul F, Aktas O, et al. MOG encephalomyelitis: international recommendations on diagnosis and antibody testing. *J Neuroinflammation*. 2018;15(1):134. doi:10.1186/s12974-018-1144-2.
3. Hardy TA, Chataway J. Tumefactive demyelination: an approach to diagnosis and management. *J Neurol Neurosurg Psychiatry*. 2013;84(9):1047-1053. doi:10.1136/jnnp-2012-304498.
4. Lucchinetti CF, Gavrilova RH, Metz I, et al. Clinical and radiographic spectrum of pathologically confirmed tumefactive multiple sclerosis. *Brain*. 2008;131(7):1759-1775. doi:10.1093/brain/awn098.
5. Shu Y, Long Y, Wang S, et al. Brain histopathological study and prognosis in MOG antibody-associated demyelinating pseudotumor. *Ann Clin Transl Neurol*. 2019;6(2):392-396. doi:10.1002/acn3.712.
6. Kim HJ, Paul F, Lana-Peixoto MA, et al. MRI characteristics of neuromyelitis optica spectrum disorder: an international update. *Neurology*. 2015;84(11):1165-1173. doi:10.1212/WNL.0000000000001367.
7. Sinha S, Banwell B, Tucker A, Storm PB, Huh J, Lang SS. Hemicraniectomy and externalized ventricular drain placement in a pediatric patient with myelin

oligodendrocyte glycoprotein-associated tumefactive demyelinating disease. *Childs Nerv Syst*. 2022;38(1):185-189. doi:10.1007/s00381-021-05139-2.
8. Budny J, Vakharia K, Kamal H, Atwal G. Transtentorial herniation from tumefactive multiple sclerosis mimicking primary brain tumor. *Surg Neurol Int*. 2018;9(1):208. doi:2018/11/3010.4103/sni.sni_131_18.
9. Fereidan-Esfahani M, Decker PA, Eckel Passow JE, Lucchinetti CF, Flanagan EP, Tobin WO. Population-based incidence and clinico-radiological characteristics of tumefactive demyelination in Olmsted County, Minnesota, United States. *Eur J Neurol*. 2022;29(3):782-789. doi:10.1111/ene.15182.
10. Cacciaguerra L, Meani A, Mesaros S, et al. Brain and cord imaging features in neuromyelitis optica spectrum disorders. *Ann Neurol*. 2019;85(3):371-384. doi:10.1002/ana.25411.
11. Banks SA, Morris PP, Chen JJ, et al. Brainstem and cerebellar involvement in MOG-IgG-associated disorder versus aquaporin-4-IgG and MS. *J Neurol Neurosurg Psychiatry*. 2020;92(4):384-390. doi:10.1136/jnnp-2020-325121.
12. Abou Zeid N, Pirko I, Erickson B, et al. Diffusion-weighted imaging characteristics of biopsy-proven demyelinating brain lesions. *Neurology*. 2012;78(21):1655-1662. doi:10.1212/WNL.0b013e3182574f66.
13. Jeong IH, Kim SH, Hyun JW, Joung A, Cho HJ, Kim HJ. Tumefactive demyelinating lesions as a first clinical event: clinical, imaging, and follow-up observations. *J Neurol Sci*. 2015;358(1-2):118-124. doi:10.1016/j.jns.2015.08.034.
14. Lopez-Chiriboga AS, Majed M, Fryer J, et al. Association of MOG-IgG serostatus with relapse after acute disseminated encephalomyelitis and proposed diagnostic criteria for MOG-IgG-associated disorders. *JAMA Neurol*. 2018;75(11):1355-1363. doi:10.1001/jamaneurol.2018.1814.
15. Wingerchuk DM, Banwell B, Bennett JL, et al. International consensus diagnostic criteria for neuromyelitis optica spectrum disorders. *Neurology*. 2015;85(2):177-189. doi:10.1212/WNL.0000000000001729.
16. Thompson AJ, Banwell BL, Barkhof F, et al. Diagnosis of multiple sclerosis: 2017 revisions of the McDonald criteria. *Lancet Neurol*. 2018;17(2):162-173. doi:10.1016/S1474-4422(17)30470-2.
17. Sechi E, Buciuc M, Pittock SJ, et al. Positive predictive value of myelin oligodendrocyte glycoprotein autoantibody testing. *JAMA Neurol*. 2021;78(6):741-746. doi:10.1001/jamaneurol.2021.0912.
18. Waters PJ, McKeon A, Leite MI, et al. Serologic diagnosis of NMO: a multicenter comparison of aquaporin-4-IgG assays. *Neurology*. 2012;78(9):665-671; discussion 669. doi:10.1212/WNL.0b013e318248dec1.
19. Redenbaugh V, Montalvo M, Sechi E, et al. Diagnostic value of aquaporin-4-IgG live cell based assay in neuromyelitis optica spectrum disorders. *Mult Scler J Exp Transl Clin*. 2021;7(4):205521732110526. doi:10.1177/20552173211052656.
20. Kurtzke JF. Rating neurologic impairment in multiple sclerosis: an expanded disability status scale (EDSS). *Neurology*. 1983;33(11):1444-1452. doi:10.1212/wnl.33.11.1444.
21. Filippi M, Preziosa P, Banwell BL, et al. Assessment of lesions on magnetic resonance imaging in multiple sclerosis: practical guidelines. *Brain*. 2019;142(7):1858-1875. doi:10.1093/brain/awz144.
22. Llufriu S, Pujol T, Blanco Y, et al. T2 hypointense rims and ring-enhancing lesions in MS. *Mult Scler*. 2010;16(11):1317-1325. doi:10.1177/1352458510377905.
23. Hardy TA, Tobin WO, Lucchinetti CF. Exploring the overlap between multiple sclerosis, tumefactive demyelination and Balo's concentric sclerosis. *Mult Scler*. 2016;22(8):986-992. doi:10.1177/1352458516641776.
24. Seewann A, Enzinger C, Filippi M, et al. MRI characteristics of atypical idiopathic inflammatory demyelinating lesions of the brain : a review of reported findings. *J Neurol*. 2008;255:1-10. doi:10.1007/s00415-007-0754-x.
25. Jurynczyk M, Geraldes R, Probert F, et al. Distinct brain imaging characteristics of autoantibody-mediated CNS conditions and multiple sclerosis. *Brain*. 2017;140(3):617-627. doi:10.1093/brain/aww350.
26. Schaefer PW, Grant PE, Gonzalez RG. Diffusion-weighted MR imaging of the brain. *Radiology*. 2000;217(2):331-345. doi:10.1148/radiology.217.2.r00nv24331.
27. Ito S, Mori M, Makino T, Hayakawa S, Kuwabara S. "Cloud-like enhancement" is a magnetic resonance imaging abnormality specific to neuromyelitis optica. *Ann Neurol*. 2009;66(3):425-428. doi:10.1002/ana.21753.
28. Poser S, Luer W, Bruhn H, Frahm J, Bruck Y, Felgenhauer K. Acute demyelinating disease. Classification and non-invasive diagnosis. *Acta Neurol Scand*. 1992;86(6):579-585. doi:10.1111/j.1600-0404.1992.tb05490.x.
29. Sanchez P, Meca-Lallana V, Barbosa A, Manzanares R, Palmi I, Vivancos J. Tumefactive demyelinating lesions of 15 patients: clinico-radiological features, management and review of the literature. *J Neurol Sci*. 2017;381:32-38. doi:10.1016/j.jns.2017.08.005.
30. Zhao-Fleming HH, Valencia Sanchez C, Sechi E, et al. CNS demyelinating attacks requiring ventilatory support with myelin oligodendrocyte glycoprotein or aquaporin-4 antibodies. *Neurology*. 2021;97(13):e1351-e1358. doi:10.1212/WNL.0000000000012599.
31. Lopez-Chiriboga AS, Sechi E, Buciuc M, et al. Long-term outcomes in patients with myelin oligodendrocyte glycoprotein immunoglobulin G-associated disorder. *JAMA Neurol*. 2020;77(12):1575-1577. doi:10.1001/jamaneurol.2020.3115.
32. Marignier R, Hacohen Y, Cobo-Calvo A, et al. Myelin-oligodendrocyte glycoprotein antibody-associated disease. *Lancet Neurol*. 2021;20(9):762-772. doi:10.1016/S1474-4422(21)00218-0.
33. Lin X, Yu WY, Liauw L, et al. Clinicoradiologic features distinguish tumefactive multiple sclerosis from CNS neoplasms. *Neurol Clin Pract*. 2017;7(1):53-64. doi:10.1212/CPJ.0000000000000319.
34. Jurynczyk M, Messina S, Woodhall MR, et al. Clinical presentation and prognosis in MOG-antibody disease: a UK study. *Brain*. 2017;140(12):3128-3138. doi:10.1093/brain/awx276.
35. Dobson R, Ramagopalan S, Davis A, Giovannoni G. Cerebrospinal fluid oligoclonal bands in multiple sclerosis and clinically isolated syndromes: a meta-analysis of prevalence, prognosis and effect of latitude. *J Neurol Neurosurg Psychiatry*. 2013;84(8):909-914. doi:10.1136/jnnp-2012-304695.
36. Algahtani H, Shirah B, Alassiri A. Tumefactive demyelinating lesions: a comprehensive review. *Mult Scler Relat Disord*. 2017;14:72-79. doi:10.1016/j.msard.2017.04.003.
37. Metz I, Gavrilova RH, Weigand SD, et al. Magnetic resonance imaging correlates of multiple sclerosis immunopathological patterns. *Ann Neurol*. 2021;90(3):440-454. doi:10.1002/ana.26163.
38. Bruck W, Bitsch A, Kolenda H, Bruck Y, Stiefel M, Lassmann H. Inflammatory central nervous system demyelination: correlation of magnetic resonance imaging findings with lesion pathology. *Ann Neurol*. 1997;42(5):783-793. doi:10.1002/ana.410420515.
39. Tham M, Frischer JM, Weigand SD, et al. Iron heterogeneity in early active multiple sclerosis lesions. *Ann Neurol* 2021;89(3):498-510. doi:10.1002/ana.25974.
40. Ordidge RJ, Gorell JM, Deniau JC, Knight RA, Helpern JA. Assessment of relative brain iron concentrations using T2-weighted and T2*-weighted MRI at 3 Tesla. *Magn Reson Med*. 1994;32:335-341. doi:10.1002/mrm.1910320309.
41. Sechi E, Krecke KN, Messina SA, et al. Comparison of MRI lesion evolution in different central nervous system demyelinating disorders. *Neurology*. 2021;97(11):e1097-e1109. doi:10.1212/WNL.0000000000012467.
42. Kim SH, Huh SY, Hyun JW, et al. A longitudinal brain magnetic resonance imaging study of neuromyelitis optica spectrum disorder. *PLoS One*. 2014;9:e108320. doi:10.1371/journal.pone.0108320.
43. Hoftberger R, Guo Y, Flanagan EP, et al. The pathology of central nervous system inflammatory demyelinating disease accompanying myelin oligodendrocyte glycoprotein autoantibody. *Acta Neuropathol*. 2020;139(5):875-892. doi:10.1007/s00401-020-02132-y.
44. Lucchinetti CF, Mandler RN, McGavern D, et al. A role for humoral mechanisms in the pathogenesis of Devic's neuromyelitis optica. *Brain*. 2002;125(7):1450-1461. doi:10.1093/brain/awf151.
45. Lucchinetti CF, Popescu BF, Bunyan RF, et al. Inflammatory cortical demyelination in early multiple sclerosis. *N Engl J Med*. 2011;365(23):2188-2197. doi:10.1056/NEJMoa1100648.
46. Lassmann H. Tumefactive multiple sclerosis or inflammatory demyelinating disease with large lesions? *Eur J Neurol*. 2022;29(3):687-688. doi:10.1111/ene.15210.